Journal of ELECTRONIC MATERIALS, Vol. 43, No. 4, 2014
DOI: 10.1007/s11664-014-3050-4
© 2014 TMS

Comparative DC Characteristic Analysis of AlGaN/GaN HEMTs Grown on Si(111) and Sapphire Substrates by MBE

PARTHA MUKHOPADHYAY,[1,5] ANKUSH BAG,[1] UMESH GOMES,[1] UTSAV BANERJEE,[4] SAPTARSI GHOSH,[1] SANJIB KABI,[1] EDWARD Y.I. CHANG,[2] AMIR DABIRAN,[3] PETER CHOW,[3] and DHRUBES BISWAS[4]

1.—Advanced Technology Development Center, IIT Kharagpur, Kharagpur 721302, India. 2.—Department of Material Science and Engineering, NCTU, Hsinchu, Taiwan. 3.—SVT Associates Inc., 7620 Executive Dr., Minneapolis, MN 55344, USA. 4.—Department of Electronics & Electrical Communication Engineering, IIT Kharagpur, Kharagpur, India. 5.—e-mail: mukhopadhyay.partha@gmail.com

A comparative assessment of AlGaN/GaN high-electron-mobility transistors (HEMTs) grown by molecular beam epitaxy on silicon and sapphire substrates has been carried out. Large-area power GaN HEMTs with identical device dimensions were fabricated on both substrates. A thicker AlN buffer layer was used for the GaN HEMT on silicon to achieve similar quality and uniformity of GaN epitaxy for rational comparison with that grown on sapphire. Direct-current analysis and physical characterization were carried out to understand the performance of the devices. Mathematical measurement of the instability of the current–voltage (*I*–*V*) characteristic at high applied drain bias was carried out to evaluate the performance of both devices. An improved two-dimensional (2D) analysis of the *I*–*V* characteristic was performed from a thermal perspective including appropriate scattering effects on the 2D electron gas mobility. The experimental and analytical studies were correlated to reveal the effects of temperature-sensitive scattering phenomena on the mobility as well as on the *I*–*V* characteristic at high drain bias in terms of lattice thermal heating. It is observed that the HEMT on Si has improved stability compared with sapphire due to its weaker scattering phenomena at high drain bias, associated with its thermal conductivity. Simulation of 2D thermal mapping was also carried out to distinguish the hot-spot regions of the devices. The comparable electrical performance of these devices illustrates the viability of AlGaN/GaN HEMTs on Si(111) to achieve low-cost stable devices with better thermal power handling for high-voltage applications.

Key words: HEMT, MBE, current slump, transconductance, linearity, breakdown voltage

INTRODUCTION

AlGaN/GaN HEMTs have been widely acknowledged for use in high-frequency, high-power, and high-temperature applications because of their features such as wide bandgap, high breakdown voltage (BV), high thermal conductivity, and transport properties. The limited availability of native GaN substrates makes commercially available sapphire a prominent substrate for GaN epitaxy.[1] Silicon is an alternative substrate, promising low cost, good thermal conductivity, large wafer area, and integration with silicon technology.[2,3] The potential integration of GaN high-power devices with advanced Si electronics is one of the main upcoming state-of-the-art technologies. Integration of GaN on silicon makes it suitable for achieving system on

(Received April 12, 2013; accepted January 21, 2014; published online February 15, 2014)

heterogeneous chip on wafer (SOHCOW) technology. The use of silicon also removes the dependence of GaN technology on sapphire, which has higher cost, smaller wafer size, and lower thermal conductivity, limiting the power performance.[4] However, the large difference in lattice constant and the thermal expansion coefficient mismatch between GaN and silicon make such integration more challenging.[5]

In this article, we report on the fabrication and performance of AlGaN/GaN HEMTs grown on silicon (111) and *c*-plane sapphire substrates. Most previous works on such comparative study between Si and sapphire HEMTs were carried out without clearly mentioning the structure/growth strategies or on dissimilar structures.[6–8] To enable fair comparative analysis of the device performance on these two types of substrate, devices with similar dimensions were fabricated and processed. To compensate for the high lattice mismatch and thermal strain in the HEMT on silicon as compared with the HEMT on sapphire, the AlN buffer layer was grown thicker in the former case. This helps to improve the quality of the GaN on the silicon substrate to attain a root-mean-square (RMS) roughness similar to that of the GaN on sapphire. This feature makes the comparison more reliable for assessment of silicon as an alternative substrate. Comparable epitaxial quality of the GaN layer on both substrates is observed in cathodoluminescence (CL), x-ray diffraction (XRD), and Hall measurements. Room-temperature direct-current (DC) characterization, including drain current, transconductance, linearity, leakage current, BV, and output power, was carried out on the silicon and sapphire samples. The current slump was calculated for different drain biases to determine the device stability. An appropriate scattering-dominated 2D electron gas (2DEG) mobility model is used to calculate the current–voltage characteristic. The experimentally determined device stability at high drain bias is further correlated with analytical results and found to be similar in nature. To explain the difference in electron mobility, technology computer-aided design (TCAD) simulation was also performed using lattice heating models. An insight into hot-spot formation is provided for both devices. Improved stability is observed for the HEMT on Si compared with sapphire due to its weaker scattering phenomena at high drain bias associated with its thermal conductivity. Furthermore, these large-area devices show high transconductance and linearity, making them suitable for use in low-cost high-power applications.

DEVICE FABRICATION

Molecular beam epitaxy (MBE; SVT Associates Inc., Minneapolis, MN) with a nitrogen radiofrequency (RF) plasma source was used to grow AlGaN/GaN heterostructures on 2-inch (111)-oriented intrinsic Si substrate and 2-inch sapphire (0001) substrate. The epitaxial structure is shown in Fig. 1. *In situ* high-temperature (~1010°C) Ga treatment was applied to remove oxides from the Si substrate, while Al_2O_3 was cleaned at a much lower substrate temperature. A nice 7 × 7 reflection high-energy electron diffraction (RHEED) reconstruction pattern was observed on the cleaned Si(111) substrate. The epilayers grown on the AlN nucleation layer were identical in both cases, as shown in Fig. 1. A nucleation layer of 0.3 μm was grown on the Si substrate in two stages. A thin high-temperature AlN layer was grown, followed by a thick AlN layer at lower substrate temperature. On the nucleation layer, a thick GaN buffer of 1.5 μm was grown. Details of the growth of the AlGaN/GaN HEMT on Si can be found in a previous publication by the authors.[9]

The GaN buffer was partially doped with Fe to increase its resistivity. The buffer growth has been observed with nice, bright, and streaky *in situ* 2 × 2 RHEED reconstruction in gallium-rich condition. A conventional 2-nm GaN and undoped 20-nm AlGaN heterojunction was grown on the buffer. The Al mole fraction was determined to be m = 0.3 by *in situ* CL and XRD experiments on both samples. These crack-free structures possess reduced tensile strain and good surface roughness (0.75 nm for Si and 0.6 nm for sapphire sample, as determined by atomic force microscopy). At room temperature, Hall measurements (Nanometrics, Milpitas, CA) on van der Pauw samples gave the 2DEG density, sheet resistivity, and mobility of the Si and sapphire sample as 1.25×10^{13} cm^{-2}, 470 Ω/sq, and 1150 cm^2/V s and 1.1×10^{13} cm^{-2}, 299 Ω/sq, and 1340 cm^2/V s, respectively, while the same at 77 K were 1.1×10^{13} cm^{-2}, 130 Ω/sq, and 3280 cm^2/V s[9] and 8.4×10^{12} cm^{-2}, 105 Ω/sq, and 4130 cm^2/V s. The high mobility at cryogenic temperature signifies that the obtained carrier density is the same as the 2DEG carrier density.[9] This means that the background impurities are frozen at low temperature, thus the charge density decreases and the mobility increases

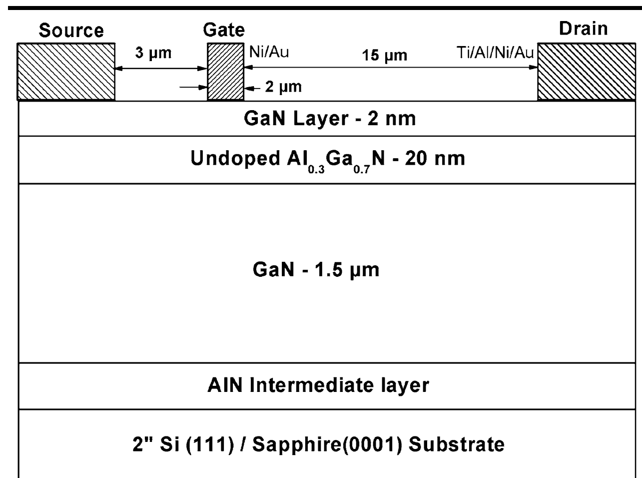

Fig. 1. Undoped AlGaN/GaN HEMT epilayers with device dimensions.

as the scattering decreases. Device fabrication consisted of conventional HEMT large-area lithography processes. After mesa etching, ohmic contacts were prepared by evaporating Ti/Al/Ni/Au layers, followed by annealing at 900°C for 30 s in N_2 environment. The Schottky gate metallization consisted of patterning a Ni/Au layer by e-beam lithography. Unpassivated double-finger devices with large source–drain separation of 20 μm, gate length of 2 μm, and gate width of 50 μm were prepared with gate–source separation of 3 μm and gate–drain separation of 15 μm.

RESULTS AND DISCUSSION

The identical device structures allow us to compare the device performance in terms of buffer quality when grown on different substrates. As the AlGaN/GaN heterojunction is undoped, the 2DEG channel is formed by spontaneous and piezoelectric polarization charges. The mobility and 2DEG concentration, for undoped AlGaN, are functions of piezoelectric coefficients, elastic constants, dislocations, and active layer thickness. As both devices have identical active layers, it can be said that the electron mobility is limited by different scattering mechanisms. Among them, buffer layer defect scattering, or more specifically dislocation scattering,[10] may dominate the degradation of the mobility in the Si sample. Figure 2 shows a comparison of *in situ* CL on a logarithmic scale. The two curves are in very close proximity, revealing the similar crystal quality of the top layer of the two samples.

A full-width at half-maxima (FWHM) of 8.07 nm with a peak at 366.07 nm was determined for the GaN buffer layer in the Si sample[9] as compared with a FWHM of 6.52 nm for the sapphire sample with a peak at 365.17 nm. These GaN layer peaks at different wavelengths indicate that the HEMT on Si may have a slightly strained GaN layer with reduced bandgap compared with normal, as it changes (conduction-band and valance-band extrema shifts) under the influence of the strain field.[11] XRD (Jordan Valley, Durham, England) analysis showed that, for the Si sample, the FWHM of the GaN (002) peak was 446 arcsec whereas the same for the sapphire sample was 129 arcsec. In summary, the sapphire sample has better crystallinity than the Si sample and the peak values of saturation current (I_{DS}) and transconductance (g_m) of the sapphire HEMT should be higher than for the Si sample, as described in the following sections.

DC characterization was carried out using a semiconductor characterization system (Keithley, Cleveland, OH). The static output characteristics of the HEMTs at different V_{GS} values from +2 V to -5 V with $\Delta V_{GS} = -1$ V at drain voltages of 0 V to 15 V on devices with 2-μm gate length are shown in Fig. 3. Drain saturation currents (I_{DS}) of 608 mA/mm for the unpassivated Si HEMT and 623 mA/mm for the unpassivated sapphire HEMT were obtained at +2 V bias on the gate.

It is observed from Fig. 3 that the stability of the HEMT on the Si substrate is retained to significantly higher DC power compared with the sapphire sample.[7] Based on our observations made at higher drain voltage (~15 V for sapphire, 20 V for Si), the drain current decreases significantly in the sapphire sample because of the self-heating effect. On the other hand, a stable I_{DS}–V_{DS} characteristic is observed at saturation due to better heat dissipation in the Si sample. This is mainly attributed to the higher thermal conductivity of Si compared with sapphire ($\kappa_{Si}/\kappa_{sapphire} = 5$).[7]

We calculated the rate of saturation drain current (I_{DSS}) slump with V_{DS}, i.e., R_{I_D}, as

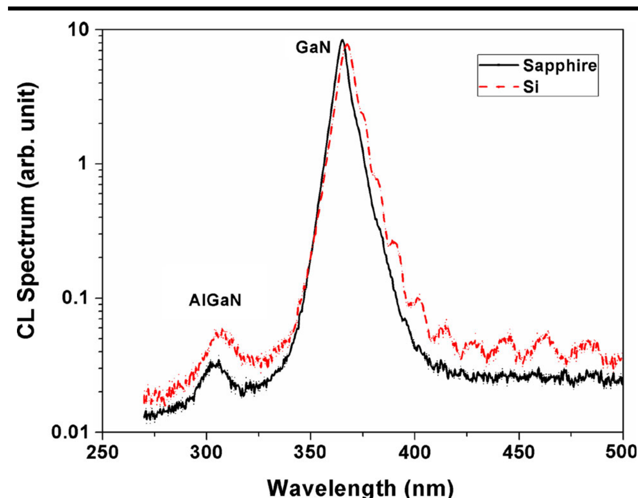

Fig. 2. Comparison of *in situ* cathodoluminescence spectra at 300 K.

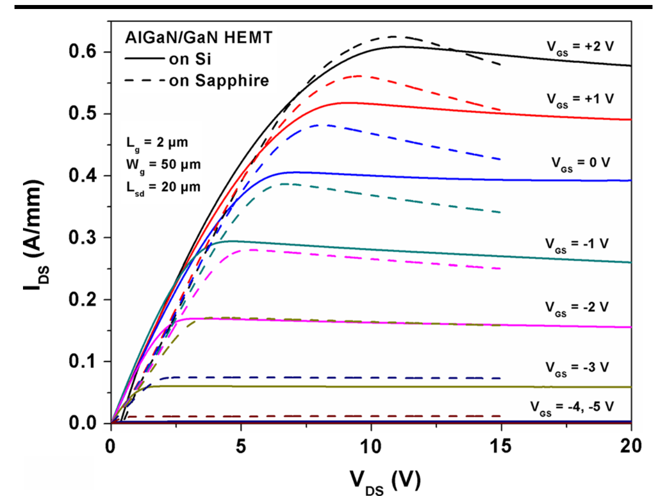

Fig. 3. Static *I–V* characteristics of 2-μm, undoped, unpassivated AlGaN/GaN HEMTs grown on Si and sapphire substrates.

$$R_{I_D} = \frac{|I_{DSS} - I_{D_{@V_{DH}}}|}{|V_{DH} - V_{D_{@I_{DSS}}}|}; \tag{1}$$

whereV_{DH} is the highest applied drain voltage:

The calculated results are shown in Fig. 4, keeping V_{DH} constant at 15 V. A lower value of R_{I_D} indicates a higher stability of the device at a particular V_{GS}. At higher negative gate voltage, lower R_{I_D} was observed for HEMTs on both Si and sapphire. We also deduced R_{I_D} theoretically by using an improved 2DEG current–voltage analytical model with a thermal perspective, as described in the following section. We found that the experimental and analytical R_{I_D} values were similar for both samples.

The HEMT device on Si showed very high stability with a current reduction rate (R_{I_D}) of 1 mA/mm V at V_{GS} = 0 V, even at V_{DS} of 20 V, as shown in Fig. 4. Therefore, the GaN power HEMT on Si is a perfect candidate for opamp cum power amplifier applications which need high stability in a high voltage range. However, both HEMTs (on Si and sapphire) can be considered for use as power switches in power converter or envelope tracking systems in RF applications because of the selective operating region (cutoff and active region) in the I_{DS}–V_{DS} characteristic.

Our analytical study, to deduce the 2DEG sheet carrier concentration, was based on self-consistent solution of the one-dimensional (1D) Poisson and Schrödinger equations, as is well documented in research articles.[12–18] To consider the effect of lattice temperature on material and transport parameters, we incorporated the lattice heat flow equation in addition to the continuity and Poisson equations, as expressed below:[19]

$$c_t \frac{\partial T_L}{\partial t} = \nabla(\kappa \nabla T_L + H), \tag{2}$$

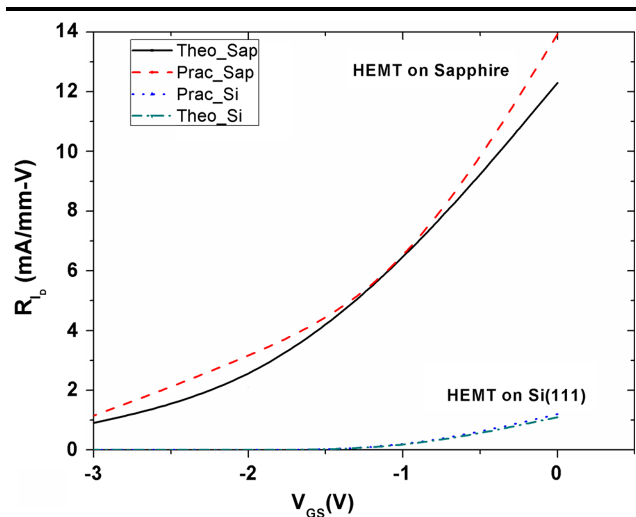

Fig. 4. Current slump rate at V_{DH} of 15 V for 2-μm, undoped, unpassivated AlGaN/GaN HEMTs.

where c_t is the heat capacitance per unit volume, κ is the thermal conductivity, H is the generated heat, and T_L is the local lattice temperature. We incorporated different temperature-dependent scattering effects into the mobility model to deduce the current–voltage relation, which can properly represent the experimentally obtained I–V curves. In the 2DEG of the AlGaN/GaN HEMTs, four main scattering mechanisms are impurity (μ_i), polar optical (μ_{po}), piezoelectric (μ_{pie}), and deformation potential acoustic phonon scattering (μ_{dpa}). We took the theoretical expressions for these from Shur et al.[20]

Though the electron gas in the quantum wells only has freedom of in-plane motion, the electron wavefunctions have finite extent in the direction of quantization, especially at high lattice temperatures generated at high applied fields. This penetration of the wavefunction into the barrier introduces alloy scattering,[21] which is also included in our study based on Eq. 3.

$$\frac{1}{\mu_{alloy}} = \frac{m_n^*}{q} \times \frac{1}{\tau_{alloy}} = \frac{(m_n^*)^2}{q\hbar^3}\Omega(m)\Delta V^2 m(1-m) \times \int_{-\infty}^{0} \psi^4(z)\, dz, \tag{3}$$

where m is the Al mole fraction, $\Omega(m)$ is the volume associated with each Al (Ga) atom, and ΔV is the alloy scattering potential due to replacement of a Ga atom by an Al atom. Beyond the saturation region at high drain voltages, accumulated lattice heat causes the electron wavefunction to spread into the barrier region.[22] This effect is more prominent in the sapphire sample owing to its lower thermal conductivity. Also, the heterojunction between AlGaN and GaN is usually a nonabrupt interface, which leads to interface roughness scattering for electrons as they move to the 2DEG.[23] In addition, lattice vibrations, generated by lattice heat accumulation at high fields, increase the interface-related scattering, especially in polar materials.[21] This effect is again higher in the sapphire sample at high applied bias. The scattering rate for interface roughness can be calculated by Fermi's Golden Rule,[24] and the corresponding mobility (μ_{IFRS}) can be written as

$$\frac{1}{\mu_{IFRS}} = \frac{m_n^*}{q} \times \frac{1}{\tau_{IFRS}} = \frac{\Delta^2 L^2 e^4 (m_n^*)^2}{2q\varepsilon^2\hbar^3}\left(\frac{1}{2}n_{2D}\right)^2 \int_0^1 \frac{u^4 e^{-k_F^2 L^2 u^2}}{\left(u + G(u)\frac{q_{TF}}{2k_F}\right)^2 \sqrt{1-u^2}}\, du, \tag{4}$$

where Δ is the root-mean-square roughness of height, L is the correlation length, q_{TF} is the Thomas–Fermi screening wavevector for the 2DEG, and $G(u)$ is a form factor that arises due to the finite extension of the 2DEG wavefunction in the growth direction. Here, $u = q/2k_F$ is used to make

the integral dimensionless. So, the overall mobility can be deduced as

$$\frac{1}{\mu(T)} = \frac{1}{\mu_{\mathrm{i}}} + \frac{1}{\mu_{\mathrm{po}}} + \frac{1}{\mu_{\mathrm{pie}}} + \frac{1}{\mu_{\mathrm{dpa}}} + \frac{1}{\mu_{\mathrm{alloy}}} + \frac{1}{\mu_{\mathrm{IFRS}}}. \quad (5)$$

In the highly degenerate 2DEG of AlGaN/GaN heterostructures, alloy scattering (μ_{alloy}) is strong due to the high electron effective mass and very high 2DEG carrier density, in spite of the confinement of the 2DEG in binary semiconductors.[23] Even the AlN/GaN heterojunction suffers from alloy scattering. The high 2DEG density also causes considerable interface roughness scattering, since the 2DEG tends to shift closer to the interface as the carrier density increases. It has been seen that the mobility decreases with increasing 2DEG density,[25] which suggests that the μ_{alloy} and μ_{IFRS} scattering mechanisms dominate the overall mobility. Increasing the 2DEG density leads to greater penetration of the electron wavefunction into the alloy barrier, and the same alloy composition experiences stronger scattering.[23] Hence, it can be said that, at high channel temperature, where the 2DEG density increases, scattering is intensified and consequently the mobility is decreased;[26] in fact, it approaches the limit set by optical phonon scattering at high temperatures.[23] The similar nature of the $R_{I_{\mathrm{D}}}$ variations in both the experimental and analytical values in Fig. 4 validates the appropriate inclusion of temperature- and mass-dependent scattering effects in the mobility model used in our analytical study. Details of the analytical model have been communicated elsewhere.[26]

To understand this phenomenon of drain current slump in AlGaN/GaN HEMTs, we performed 2D physics-based simulations using a commercial TCAD suite, Silvaco ATLAS. The polarization effects are included in the analysis by introducing a thin layer of fixed positive charge at the GaN/AlGaN interface using the polarization models. Charges due to the piezoelectric effect are also incorporated in the simulations. The GIGA module was used consistently with BLAZE to reveal the effect of lattice temperature on material and transport parameters. We configured the GIGA module as per the above-described thermal analytical model. Figure 5 shows the simulated two-dimensional temperature map of both devices, where a hot-spot region is clearly visible at the drain-side gate edge. The higher heat retention in the channel of the HEMT on sapphire has the expected effect of increased temperature at the gate drain edge. This activates the scattering mechanisms, thereby reducing the electron mobility. This thermal profile is further helpful in analyzing electrical properties such as the drain current stability and transconductance.

The transfer characteristics of unpassivated AlGaN/GaN HEMTs on Si and sapphire are shown

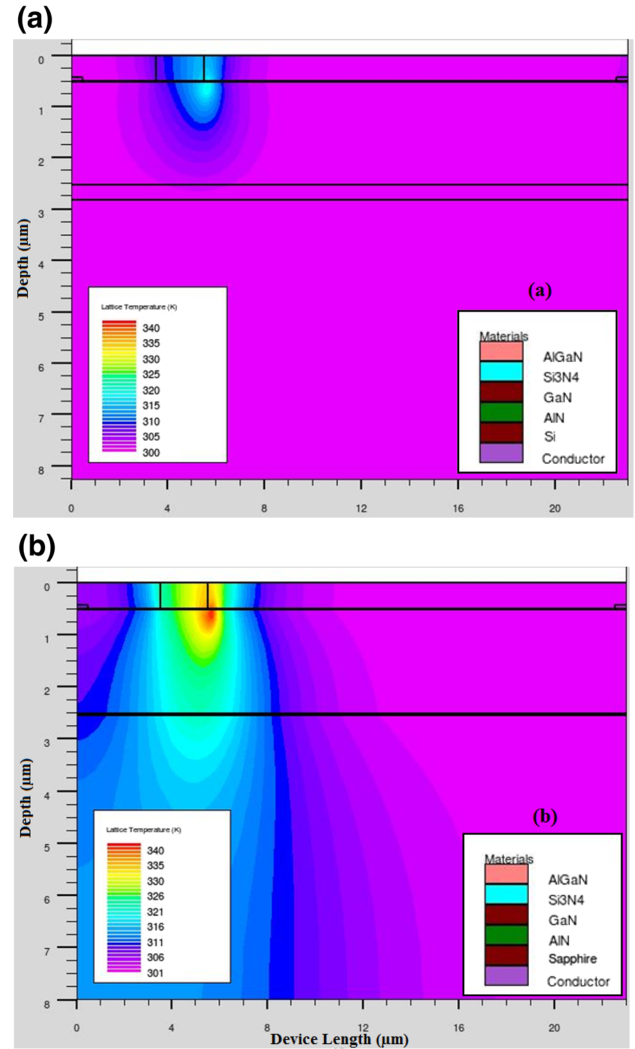

Fig. 5. Thermal profile of GaN HEMTs on (a) silicon and (b) sapphire substrates.

in Fig. 6. Peak transconductance (g_{m}) of 105 mS/mm was measured for the Si sample and 115 mS/mm for the sapphire sample with longer gate length of 2 μm and longer source–drain distance of 20 μm. However, further enhancement can be achieved by optimizing the HEMT dimensions, especially the gate length and gate drain spacing.

Comparing the room-temperature 2DEG densities of the two samples, it can be said that the threshold voltages, V_{th}, are in close proximity, which is the case here. As per generalized observations, the V_{th} of the sapphire sample seems to be lower than that of the Si sample. However, it has been observed that the transfer characteristic of AlGaN/GaN HEMTs is a function of device operating temperature. Nuttinck et al.[27] showed that V_{th} increases with channel temperature. Due to the high channel temperature generated at high V_{DS} in the sapphire sample, the 2DEG density is increased, in turn increasing the V_{th} of the device. We also

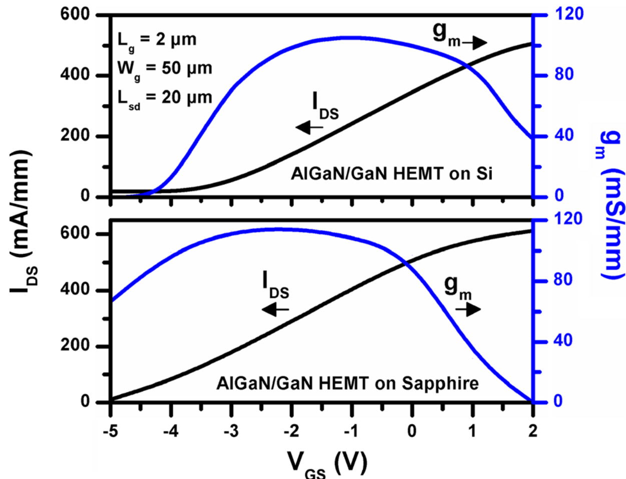

Fig. 6. Transfer characteristics and transconductance of 2-μm, undoped, unpassivated AlGaN/GaN HEMTs grown on Si and sapphire substrates.

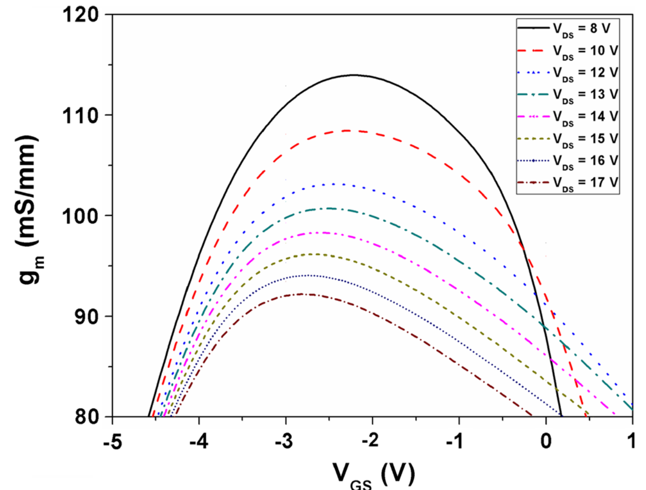

Fig. 7. Comparison of g_m curves of a 2-μm AlGaN/GaN/sapphire HEMT at different V_{DS}.

observed experimentally that increasing V_{DS} (8 V to 15 V) increases the V_{th} of the sapphire sample, similar in nature to Fig. 7, where g_m decreases with increasing V_{DS}.[27] This again proves that increasing V_{DS} increases the channel temperature, and as a result V_{th} increases. In addition, the stress generated at the high applied V_{DS} of 20 V decreases V_{th} in the Si sample.[28] This may be because of the presence of a higher threading dislocation density than in the sapphire sample, as mentioned earlier.

Figure 7 shows a comparison of the g_m curves of the HEMT on sapphire sample measured at different drain voltages. When the drain voltage is increased, the transconductance peak decreases and the peak position shifts to a more negative gate voltage. We calculated the g_m peak decrement rate with drain voltage, i.e., R_{g_m}, by following Eq. 1 as described above. In the case of the sapphire sample, the g_m peak decreased by 2.18% per unit V_{DS} increment and R_{g_m} was 2.26 mS/mm V. Analyzing Fig. 7, it can be observed that the g_m peak decreases by ~16% when V_{DS} is increased from 8 V to 15 V. This significant reduction of g_m governs the instability of the sapphire sample at higher drain voltages. On the other hand, for the Si(111) sample, R_{g_m} is 0.16 mS/mm V, so the g_m peak decreased by 0.16% per unit V_{DS} increment. This high stability of the GaN power HEMT on Si at high applied voltage indicates its suitability for use in power amplifier designs.

The ratio of the third-order sideband power to the fundamental power (IP3) is proportional to (g_m''/g_m).[29] Reduction of this ratio (to close to zero) represents improvement in the linearity of the device.[30] Figure 8 shows the variation of (g_m''/g_m) with the gate voltage. These linearity characteristic curves for the two devices are in close proximity, which explains the similar nature of their linearity.

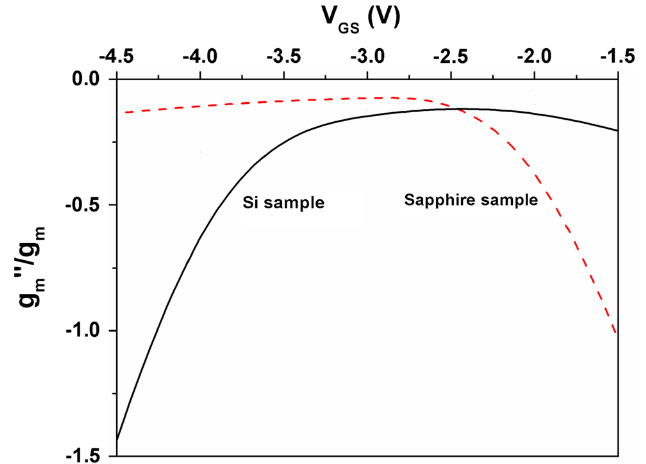

Fig. 8. Comparison of linearity between 2-μm AlGaN/GaN HEMTs on Si(111) and sapphire.

Closeness of the (g_m''/g_m) peak to zero (on the Y axis) explains the good linearity property of both HEMTs and therefore their potential as candidates for use in power amplifier designs.

I_G–V_{GS} characterization of the devices was performed over a wide range of V_{GS} from −20 V to +10 V. It was found that the sapphire sample has lower gate leakage current and much higher gate resistance than the Si sample. This result and characteristic behavior indicate the low-power applicability of the sapphire sample. Figure 9 depicts the off-state BV behavior of both devices. The sapphire sample has higher off-state BV of 60 V as compared with the Si sample (50 V), mainly because of the lower critical electric field strength (0.3 MV/cm) of Si compared with sapphire.[31] Thus, Si substrate with higher resistivity or a thicker AlN nucleation layer needs to be used[32] to improve the

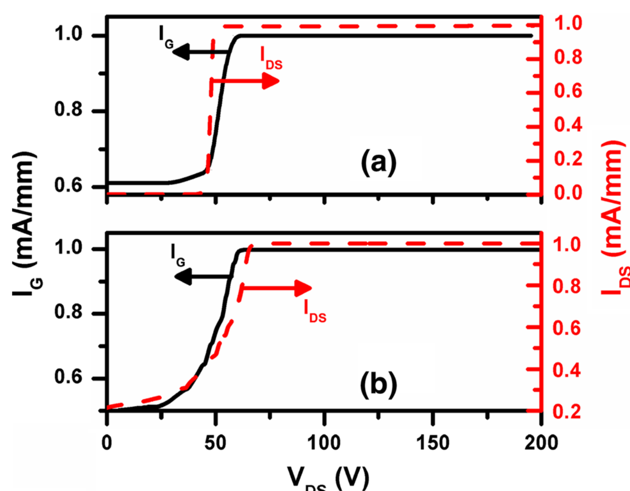

Fig. 9. Off-state breakdown voltage of (a) Si and (b) sapphire samples.

BV of such HEMT devices. High on-state BV is expected in the HEMT on Si sample due to the higher heat dissipation, hence making it suitable for high-power switching applications. The output power of the AlGaN/GaN HEMT can be estimated by calculating[33] $P_{out} = (I_{Dmax}/2) \times (V_{DS} - V_{knee})/2$ in the saturation region with V_{DS} fixed at 20 V. A stable output power of 1.73 W/mm was observed for the HEMT on Si at $V_{GS} = 0$ V, whereas the HEMT device on sapphire showed variable P_{out} at higher drain voltages when the self-heating effect is considered.

CONCLUSIONS

Undoped AlGaN/GaN heterostructures were grown on 2-inch Si(111) and sapphire substrates by MBE, being identical except for the AlN nucleation layer, which was thicker for the HEMT realized on the silicon substrate to compensate the lattice and thermal property mismatch. This helped to achieve comparable epilayer quality for both devices, making their comparison reasonable. Both unpassivated, large-area HEMT devices (L_g of 2 μm) were fabricated with identical device dimensions. Owing to the good crystalline quality of the GaN layer on the Si substrate, comparable (to the sapphire sample) 2DEG mobility with healthy drain saturation current (608 mA/mm), peak transconductance (105 mS/mm), and linearity were observed. The current slump and instability of g_m at higher drain voltages were measured analytically for both HEMT samples, and it was found that the HEMT on Si was superior. An improved, lattice-temperature-based 2D analytical model of the I–V characteristic with a mobility model dominated by different scattering mechanisms was applied. It supports the experimentally deduced instability of the electrical characteristics of the devices at high applied drain bias. It was observed that, due to the weaker scattering phenomena at high drain bias (associated with the thermal conductivity), the HEMT on Si showed better stability compared with sapphire. Continuing to an analytical model, ATLAS simulations were performed to map the hot-spot region and predict the numerical values of the channel temperature. The lower threshold voltage of the HEMT on Si makes it suitable for low-voltage device applications, whereas the lower gate leakage behavior of the HEMT on sapphire confirms its appropriateness for low-power device applications. Similar linearity and off-state BV were observed for the two transistors. The high stability, linearity, output power (1.7 W/mm), and sustainability of saturation current and g_m at high applied drain voltages for the HEMT on Si sample make it a better fit for low-cost high-power amplifier applications. Further improvement of the performance of the HEMT on Si can be achieved by increasing the resistivity of the substrate/buffer and growing a thicker AlN nucleation layer.

ACKNOWLEDGEMENTS

This work has been supported by “ENS” project, Department of Information Technology (DeitY), Government of India at Indian Institute of Technology, Kharagpur. The authors would like to thank Sounak Roy, Ashis Maity, and Amrita of IIT Kharagpur for their support.

REFERENCES

1. S. Yagi, M. Shimizu, M. Inada, Y. Yamamoto, G. Piao, H. Okumura, Y. Yano, N. Akutsu, and H. Ohashi, *Solid State Electron.* 50, 1057 (2006).
2. P. Mukhopadhyay, P. Das, E.Y. Chang, and D. Biswas, *J. Nano-Electron. Phys.* 3, 1102 (2011).
3. S. Tripathy, V.K.X. Lin, S.B. Dolmanan, J.P.Y. Tan, R.S. Kajen, L.K. Bera, S.L. Teo, M.K. Kumar, S. Arulkumaran, G.I. Ng, S. Vicknesh, S. Todd, W.Z. Wang, G.Q. Lo, H. Li, D. Lee, and S. Han, *Appl. Phys. Lett.* 101, 082110 (2012).
4. S. Arulkumaran, Z.H. Liu, G.I. Ng, W.C. Cheong, R. Zeng, J. Bu, H. Wang, K. Radhakrishnan, and C.L. Tan, *Thin Solid Films* 515, 4517 (2007).
5. P. Javorka, A. Alam, M. Marso, M. Wolter, J. Kuzmik, A. Fox, M. Heuken, and P. Kordoš, *Microelectron. J.* 34, 435 (2003).
6. P. Javorka, A. Alam, M. Wolter, A. Fox, M. Marso, M. Heuken, H. Luth, and P. Kordos, *IEEE Electron Dev. Lett.* 23, 4 (2002).
7. S. Arulkumaran, T. Egawa, and H. Ishikawa, *Solid State Electron.* 49, 1632 (2005).
8. A. Curutchet, N. Malbert, N. Labat, A. Touboul, and M. Uren, *Microelectron. Reliab.* 43, 1713 (2003).
9. P. Mukhopadhyay, S. Chowdhury, A. Wowchak, A. Dabiran, P. Chow, and D. Biswas, *J. Vac. Sci. Technol. B* 31, 03C132 (2013).
10. X.H. Wu, D. Kapolnek, E.J. Tarsa, B. Heying, S. Keller, B.P. Keller, U.K. Mishra, S.P. DenBaars, and J.S. Speck, *Appl. Phys. Lett.* 68, 1371 (1996).
11. D. Jena and U.K. Mishra, *Appl. Phys. Lett.* 80, 64 (2002).
12. M.K. Chattopadhyay and S. Tokekar, *Solid State Electron.* 50, 220 (2006).
13. X. Cheng, M. Li, and Y. Wang, *Solid State Electron.* 54, 42 (2010).
14. X.Z. Dang, P.M. Asbeck, E.T. Yu, G.J. Sullivan, M.Y. Chen, and B.T. McDermott, *Appl. Phys. Lett.* 74, 3890 (1999).
15. K. Lee, M.S. Shur, T.J. Drummond, and H. Morkoc, *IEEE Trans. Electron Dev.* 30, 207 (1983).
16. T.-H. Yu and K.F. Brennan, *IEEE Trans. Electron Dev.* 50, 2 (2003).

17. N. DasGupta and A. Dasgupta, *Solid State Electron.* 36, 201 (1993).
18. S. Kola, J.M. Golio, and G.N. Maracas, *IEEE Electron Dev. Lett.* 9, 136 (1988).
19. Y.-R. Wu and J. Singh, *J. Appl. Phys.* 101, 113712 (2007).
20. M. Shur, B. Gelmont, and M. Asif Khan, *J. Electron. Mater.* 25, 5 (1996).
21. B.R. Nag, *Physics of Quantum Well Devices* (New York: Kluwer Academic, 2002), pp. 139–172.
22. S. Mukhopadhyay and B.R. Nag, *Phys. Rev. B* 48, 17960 (1993).
23. C. Wood and D. Jena, *Polarization Effects in Semiconductors* (New York: Springer Science and Business Media, 2008), pp. 161–214.
24. D.K. Ferry and S.M. Goodnick, *Transport in Nanostructures*, 1st ed. (Cambridge: Cambridge University Press, 1999).
25. I.P. Smorchkova, L. Chen, T. Mates, L. Shen, S. Heikman, B. Moran, S. Keller, S.P. DenBaars, J.S. Speck, and U.K. Mishra, *J. Appl. Phys.* 90, 5196 (2001).
26. P. Mukhopadhyay, U. Banerjee, and D. Biswas, unpublished, communicated.
27. S. Nuttinck, B. Banerjee, S. Venkataraman, J. Laskar, and M. Harris, *IEEE MTT-S Int. Microw. Symp. Dig.* 1, 221 (2003).
28. H. Kim, R.M. Thompson, V. Tilak, T.R. Prunty, J.R. Shealy, and L.F. Eastman, *IEEE Electron Dev. Lett.* 24, 421 (2003).
29. P. Mukhopadhyay, S. Kundu, P. Das, P. Saptarshi, E.Y. Chang, and D. Biswas, *CS Mantech Technical Digest*, 51 (2010).
30. R.E. Williums and D.W. Shaw, *IEEE Trans. Electron Dev.* 25, 600 (1978).
31. P.E. Malinowski, J. Duboz, P.D. Moor, J. John, K. Minoglou, P. Srivastava, F. Semond, E. Frayssinet, B. Giordanengo, A.B. Moussa, U. Kroth, A. Gottwald, C. Laubis, R. Mertens, and C.V. Hoo, *IEEE Electron Dev. Lett.* 32, 1561 (2011).
32. S. Arulkumaran, T. Egawa, T. Matusi, and H. Ishikawa, *Appl. Phys. Lett.* 86, 123503 (2005).
33. D. Ducatteau, A. Minko, V. Hoël, E. Morvan, E. Delos, B. Grimbert, H. Lahreche, P. Bove, C. Gaquière, J.C. De Jaeger, and S. Delage, *IEEE Electron Dev. Lett.* 27, 7 (2006).